Chapter 5

Ion transport mechanism in polymer-NASICON hybrid composites

In chapters 3 and 4, we have discussed thoroughly the effect of dispersion of active fillers NASICONs (LTP, LATP, NTP, and NZSP) in respective Na^+ or Li^+ ion based solid polymer electrolyte matrix that leads to significant enhancement in the ionic conductivity. The impedance spectroscopy and other electrical investigations gave a reasonable understanding of the role of NASICONs. Nevertheless, structural features also require investigation to establish a mechanism of ion transport. Thus the current chapter discusses structural aspects of these composites, essentially to address the following:

(i) Ion chain coupling/decoupling of PEO ether oxygen with cations when compositional changes are introduced.

(ii) A generalized ion transport mechanism for Na^+ and Li^+ ion based in polymer-NASICON hybrid composites by correlating the observations from electrical transport to the structural investigations.

Thus, the chapter discusses the X-ray absorption near edge structure spectroscopy (XANES) and X-ray photoelectron spectroscopy (XPS) investigations on Na^+ and Li^+ ion polymer-NASICON hybrids.

(i) M.D. Singh, A. Dalvi, D.M. Phase, *Electrical transport in PEO-NaI-NASICON nanocomposites: An assessment using impedance and X-Ray absorption spectroscopy*, **Mater Res Bull. 118 (2019) 110485**
(ii) M. D. Singh, A. Dalvi, D M Phase, "*Novel $Na_3Zr_2Si_2PO_{12}$-polymer hybrid composites with high ionic conductivity for solid-state ionic devices*" **Materials Letters 262 (2020) 127022**
(iii) M. D. Singh, A. Dalvi, D M Phase, Y. Kumar, "*$Li_{1.3}Al_{0.3}Ti_{1.7}(PO_4)_3$ reinforced hybrid polymer composites: Assessment of enhanced Li^+ ion transport and potential for solid state supercapacitor applications*", ***J. Mat. Science*, 55 (2020) 3951–3963**
(iv) *M.D. Singh, A. Dalvi, "Ionic transport in NASICON-Polymer Hybrids: An assessment using X-ray photoelectron spectroscopy"* ***Applied Surface Science 536 (2021) 147792.***

5.1 Structural features based on XANES

In view of significant conductivity rise with NASICON content even for fixed salt content, XANES was used to examine the local structure for establishing conductivity-structure correlation.

5.1.1 Na^+ ion conducting composites:

The section presents a discussion on the following compositions

(a) 10 NaI-90[PEO1-xNTPx] where $0 \leq x \leq 0.7$, and $NaTi_2(PO_4)_3$ termed as NTP. The composite with x = 0 is abbreviated as 0 NTP, and similarly for x = 0.1 as 10 NTP and so on upto x = 0.7 as 70 NTP.

(b) 63NZSP-37($PEO_{1-x}NaI_x$) for x = 0.03–0.13, where $Na_3Zr_2Si_2PO_{12}$ is term as NZSP

At first, XANES spectra of pristine PEO was obtained and taken as a reference, particularly to examine ion coordination about ether oxygen. As discussed, ethylene oxide of PEO plays a vital role through ion-chain coupling in the ionic conduction mechanism in SPEs [1][2]. Thus, XANES spectra for O K-edge were obtained and K-edge energies were compared with respect to compositional variations.

At the outset obtained XANES spectra were processed with the ATHENA software package [3] for pre-edge background correction, and also to obtain spectral peak positions for carbon and oxygen. Thus XANES spectra of pristine PEO film were taken and the excitation energies corresponding to the K-edge of Carbon and Oxygen for various bonding were assigned. Fig. 5.1 shows the XANES spectra that correspond to normalized intensity versus energy for Oxygen (O) and Carbon (C), respectively. The K-edge energies for each transition were obtained from the peak derivative of the XANES spectra as also done by others [4][5]. The pre-edge and EXAFS portions were excluded from the present investigation due to large possible errors. As apparent in Fig. 5.1a and b, the K-edge energies in the XANES region for Oxygen and Carbon, respectively are in the range of energy values obtained previously[6][7].

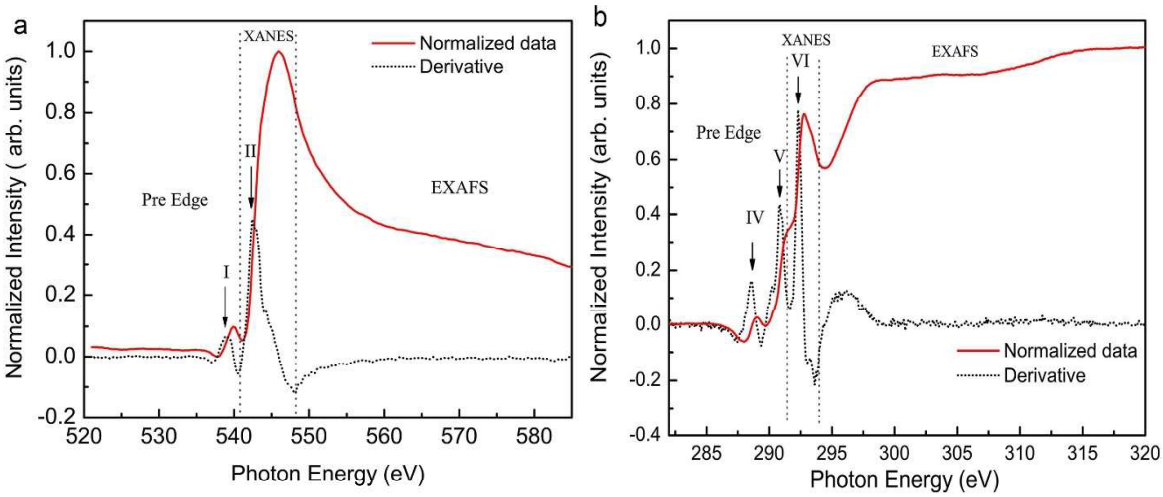

Figure 5.1 *(a) Normalized XANES spectra for Oxygen (O) K-edge of pristine PEO film. The marked arrow represents K-edge energy values for oxygen. (b) Normalized XANES spectra for carbon (C) K-edge of pristine PEO film. The marked arrow represents K-edge energies for carbon. Instrument resolution: 0.1 eV.*

The normalized intensity vs photon energy is plotted for O K-edge as shown in Fig. 5.2a for various NTP contents in the matrix. The peak-I corresponds to pre edge transition 1s → π* transition. Further, the peak-II corresponds to main edge 1s → σ* (i.e. 1 s to continuum) transition and its trend is important to understand the neighborhood or surroundings about the oxygen. For 10 NTP, only peak-I and II are visible which may correspond to ether oxygen of PEO. As the NTP content increases in the polymer, there appears a new peak-III, more prominently for 70 NTP that may be attributed to some state of oxygen existing in the NTP network. Thus for higher NTP content, the NTP oxygen also shows its presence that is reflected in the form of peak-III. Similarly Peak-IV, V and VI in Fig. 5.2b correspond to carbon and may be assigned to transition 1 s → σ* (i.e. continuum state) of C-H, C-C and C-O resonance. All the assigned transitions are listed in Table 1.

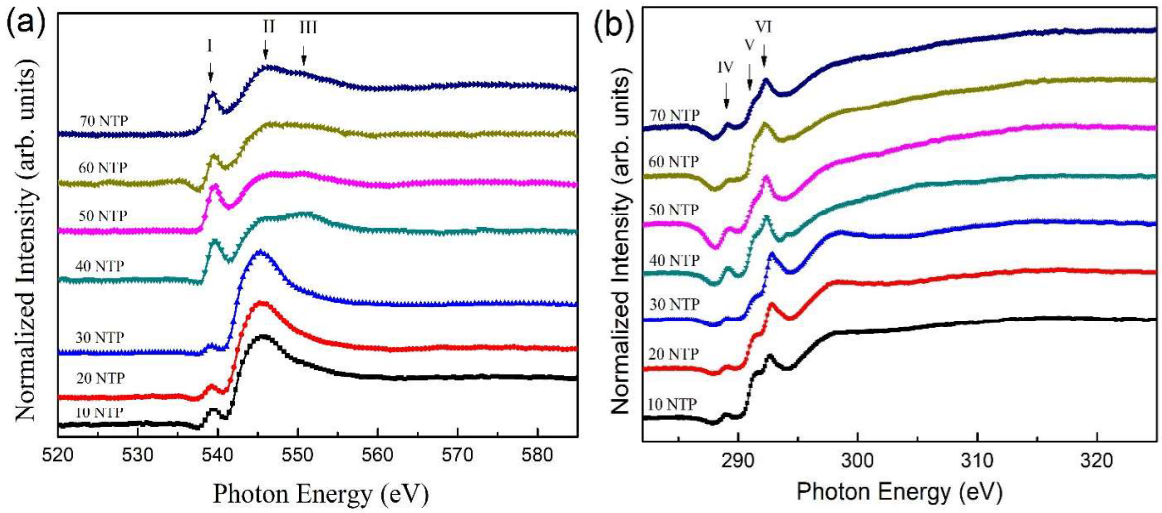

Figure 5.2 *(a) Normalized XANES spectra with NTP variation for oxygen. The peak assignment corresponding to I, II and III are given in Table 1. (b) Normalized XANES spectra with NTP variation for carbon. The peak assignment corresponding to IV, V and VI are given in Table 1. Instrument resolution: 0.1 eV.*

Table 5.1 Peak positions assigned to various excitations in XANES spectra

Peak number	Excitation energies/eV	Assignment	Reference
I	538.8	Non bonding π	[7]
II	542	Anti bonding σ*	[7]
III	549.5	NTP	Present work
IV	288.5	C-H*	[8]
V	290.8	C-C*	[8]
VI	292.3	C-O σ*	[8]

The K-edge energy values for ether oxygen are plotted with NTP content in the polymer matrix in Fig. 5.3. Further, the same is plotted for carbon in the inset. As apparent, the K-edge energy for C does not change significantly with NTP addition in the matrix. It thus suggests that NTP addition does not affect polymer backbone bonding or environment about C, as also proposed earlier [9]. However, the O K-edge energy exhibits some interesting trends as shown in Fig. 5.3. Its value increases monotonically with NTP content. Subsequently, for 50 NTP that contains 45 wt% of NTP, it tends to saturate and shows a subtle but significant drop for further

higher content i.e. 70 NTP. This may be seen in the context of decreasing O/Na ratio with NTP addition in the polymer matrix. NTP substitutes PEO and hence ether oxygen since salt content is fixed. Therefore, it is expected that the cation concentration around the ether oxygen should increase initially.

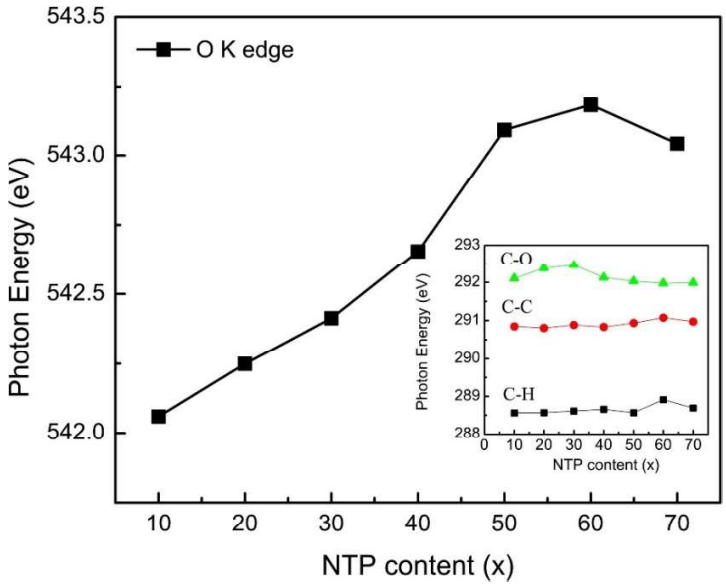

Figure 5.3 *1 s → σ* transition energy for O K-edge XANES spectra (corresponding to peak II in Fig 5.2a) versus NTP content. Inset: 1 s → σ* transition energy for carbon K-edge spectra (from peak-IV,V and VI in Fig. 5.2b**).** Instrument resolution: 0.1 eV.*

Such an increasing trend of cation concentration around ether oxygen suggests the coupling of salt ions with ether oxygen of polymer chains. For large NTP content, the concentration of cation about ether oxygen becomes very high and due to a possible concentration gradient of accumulated ions, cations tend to diffuse away from the ether oxygen. In addition, a local electric field of accumulated ions may discourage other cations to form coordination with ether oxygen. With increasing NTP content (50 – 70 NTP), therefore, cations may decouple from polymer chains. The K-edge energy for oxygen of NTP appears significantly only for higher NTP content (Fig. 5.3), its value does not show any notable shift and is not conclusive. These results, particularly (i) coupling of cations with ether oxygen for low NASICON content and (ii) decoupling at large content immensely help in understanding the conductivity structure relationship in the composites.

Based on the above investigations, the following mechanism may be suggested for ionic transport in these hybrids:

(i) For low NTP content, the concentration of ether oxygen is high, and thus cations possibly like to stay in the polymer matrix. Thus due to the high dielectric constant of NTP, the pairing of opposite charges is discouraged [9]. Thus, cations interact electrostatically with ether oxygen and establish week coordination. On application of electric field, ions move from one ether oxygen to another, shifting the coordination sites. During electrical transport, ion-chain coupling mechanisms may dominate or may play a significant role. NTP nanocrystallites though contribute in a way that their presence improves the amorphous nature of PEO. Therefore the electrical transport will only be governed by ion-chain coupling mechanism.

(ii) A moderate NTP content (E.g. 40 NTP) may affect polymer chain flexing. However, the density of cations about ether oxygen still increases as suggested by an increasing trend of the O-K edge energy (Fig. 5.3). In such a situation, ions may move through shifting the coordination with ether oxygen as well as through polymer-NASICON interface.

(iii) For very high NASICON content (50 – 70NTP), decoupling of Na^+ ions with polymer chains takes place as suggested by XANES spectra (Fig. 5.3). Since ion mobility increases noticeably (Chapter 4, Table 4.1), it may be suggested that the majority of Na^+ ions may prefer to move through the surface states of NTP at the polymer-NASICON interface. However, any diffusive motion through NASICON cannot be ascertained with these probes and more sophisticated experiments are required. A Na^+ ion to enter into bulk of NTP grain from polymer may need to cross a significant energy barrier, thus ions may prefer to move through polymer-NASICON interface. A similar possibility of transport of Na^+ ions through an interface has been suggested recently by Zhang et. al. on PEO-NaTFSI-NZMSPO system [10] where the surface percolation mechanism has been suggested.

To complement the above ion transport mechanism for higher NASICON content samples, considering the 63 % of NZSP (i.e. analogous to 70 NTP as discussed above), the effect of salt concentration on the cost of PEO is further studied using XANES.

To understand the role of the polymer matrix in ceramic in enhancing the ionic conductivity, the local structure around ether Oxygen of backbone chains $(–CH_2–CH_2–O–)_n$ was studied using synchrotron radiation. Fig. 5.4 shows normalized XANES spectra for oxygen K-edge. The main edge/white line energy (E_o) values corresponding to 1s → continuum state (i.e. 1s → 2σ* transition) were obtained from the peak derivative. Such a transition is known to be sensitive to the chemical charge state of the element. The inset of Fig. 5.4 also shows an interesting trend of the K-edge energy (E_o) values with salt content. As the salt content increases, the E_o initially shows a jump followed by an apparent saturation. It may be emphasized here that salt addition leads to a gradual decrease in O/Na ratio. Since more Na^+ ions are available for oxygen, thus it was also expected that their accumulation about ether oxygen would be leading to a gradual increase in E_o. Instead one observes no variation E_o value in a wide composition range.

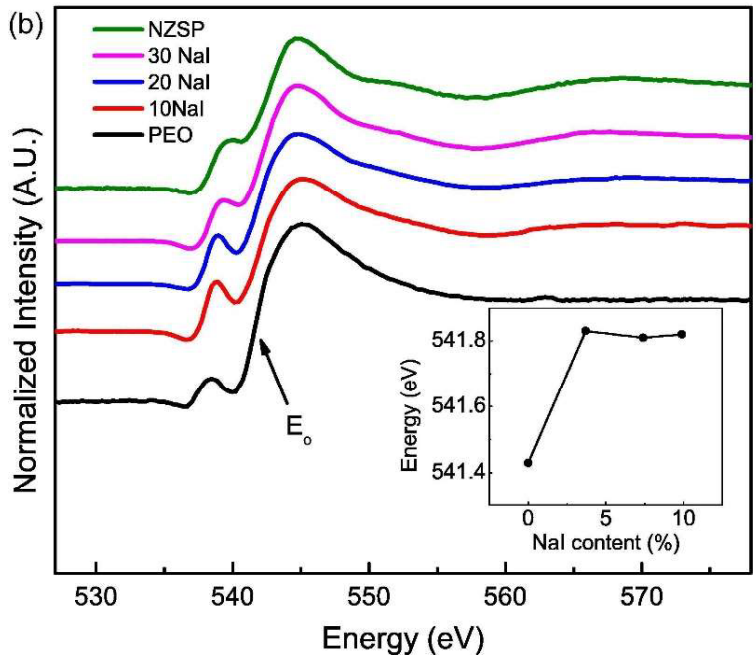

Figure 5.4 *Normalized XANES spectra processed using ATHENA software. Inset: O-K edge energy (E_o) variation with salt addition. Instrument resolution: 0.1 eV.*

This trend of E_o may be associated with a tendency of decoupling of Na^+ ions from the ether oxygen of PEO matrix. Such decoupling may enhance the mobile Na^+ ion concentration near the polymer–NZSP interface. Decoupled ions, in presence of an electric field may find

pathways either from (i) NZSP nanocrystallites, or (ii) from the surface states of NZSP through polymer–NZSP interface.

5.1.2 Li^+ ion transport in the composites

The current section discusses the composition of $5LiCF_3SO_3$-$95[PEO_{1-x}LATP_x]$, where $0 \leq x \leq 0.7$ and $Li_{1.3}Ti_{0.7}Al_{1.3}(PO_4)_3$ as LATP. In the discussion the composite with x = 0 is abbreviated as 0 LATP, similarly for x = 0.1 as 10 LATP and so on upto x = 0.7 as 70 LATP.

5a) with varied

LATP content. As apparent, O K-edge of pristine PEO shows two transition peaks. The first weak transition (I in Fig. 5.5a) may be referred to as pre-edge transition and can be assigned to core 1 s state to vacant state, i.e., 1 s $\rightarrow 2\pi^*$. Further, the second transition (II in Fig. 5.5a) is assigned to main edge or white line [11] and represents 1 s to continuum state (i.e., 1 s $\rightarrow 2\sigma^*$). Again, the transition from 1 s $\rightarrow 2\sigma^*$ is sensitive to the chemical charge state of the element due to any change in coordination, therefore, more important for the present study. The O K-edge energy (E_O) corresponding to this transition (region II) is obtained from the peak derivative [5] of the XANES spectra (inset of Fig. 5.5a for pristine PEO, 40 and 70 LATP) for each composition and plotted with varied LATP content as shown in Fig. 5.5b.

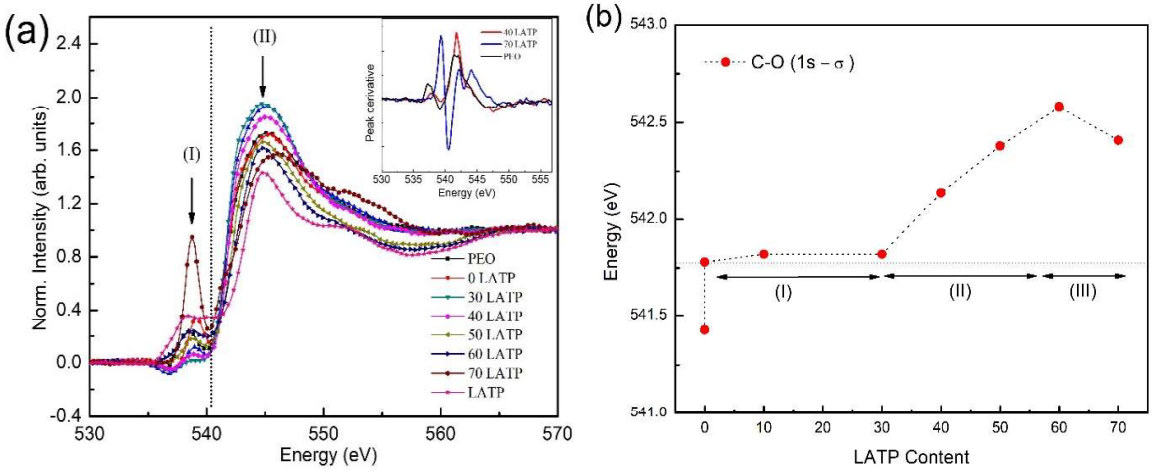

Figure 5.5 *(a) Normalized XANES spectra for O K-edge with varied LATP content. Inset shows peak derivative of XANES spectra for PEO, 40 LATP and 70 LATP sample. (b) O K-edge energy (E_O) obtained from peak derivative of XANES spectra with LATP content. Instrument resolution: 0.1 eV.*

Interestingly, E_O shows an increasing trend with composition. Firstly, when PEO is added with salt, it jumps to a higher value. This may be due to Li^+ ions from salt surrounding ether oxygen. Secondly, now when the NASICON content is added to the matrix (on cost of PEO), it almost remains constant till 30 LATP. However, a significant gradual rise in the energy is observed for 30-50 LATP content. This may be due to decrease in the O/Li ratio (Chapter 3, Table 1) that duly enhances the number of Li^+ ion availability for ether oxygen. Thus, in a way, Li^+ ion crowding about ether oxygen gives rise to strong coupling. The E_O value decreases on further increasing LATP content (for 70 LATP) that may be readily attributed to the decoupling of Li^+ ions from ether oxygen (hence polymer matrix). It may be suggested that excessive ion crowding (due to low O/Li ratio) around the ether oxygen possibly detaches Li^+ ions from chains.

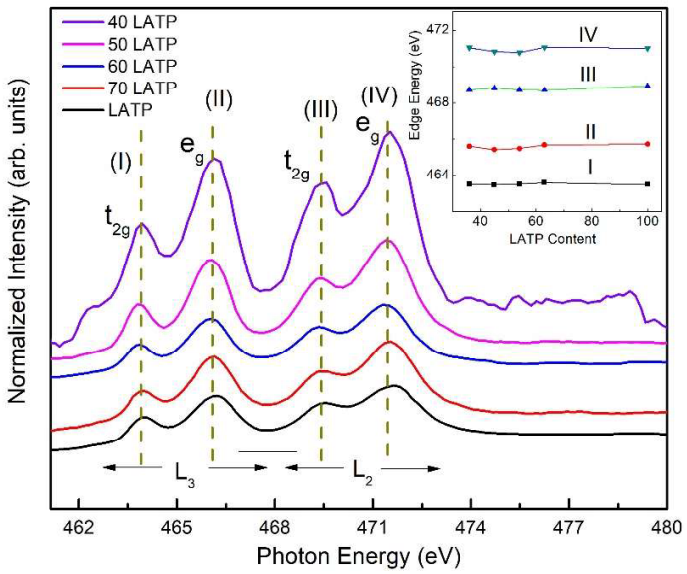

Figure 5.6 *Normalized XANES spectra for Ti L-edge with varied LATP content. Inset shows Ti L-edge energy values correspond to t_{2g} and, e.g., transition for L2 and L3 edge*

Further, to understand the in-grain structural changes of LATP due to the composite formation, the L-edge of titanium was also studied. This was investigated particularly for samples with significant amount of LATP. Fig. 5.6 shows Ti L-edge, for composites (40, 50, 60, and 70 LATP) with the bulk reference (LATP). The spectra mainly contain the L3 ($2p_{3/2}$) and L2 ($2p_{1/2}$) edges which further undergo splitting due to the crystal field (t_{2g} of Ti 3d orbital) and

(e.g., of Ti 3d orbital) corresponding to the two edges, respectively [12]. The inset of Fig. 5.6 shows edge energies with LATP content corresponding to each transition obtained from peak derivatives. Evidently, the peak positions are nearly constant with LATP and do not exhibit any apparent shift. Thus, it readily suggests that the coordination environment about Ti does not change when compositional changes in the composites.

This particular trend of the XANES spectra along with the electrical transport studies readily suggests an interesting conductivity–structure correlation that leads to a mechanism of ion transport:

(i) For 0-30 LATP samples (region I, Fig. 5.5b), as the LATP content increases (substituting PEO), the E_O value does not show any significant change. It readily suggests the almost constant number of Li^+ ions couple with ether oxygen in this composition range. In this situation, no significant rise in conductivity is observed. As the ion mobility also remains unchanged (Chapter 3, Table 3.1), it may be suggested that due to the significant crystalline phase of PEO, most of the Li^+ ions are not mobile.

(ii) In region II (30-50 LATP, Fig. 5.5b), due to the addition of LATP, the crystallinity decreases significantly (Chapter 3, Section 3.2.1). Further, a gradual decrease in the O/Li ratio enhances Li^+ ion availability for the ether oxygen. Therefore, Li^+ ion coupling with ether oxygen gradually enhances leading to an apparent rise in K-edge energy. Thus, Li^+ ions prefer to stay in the polymer matrix and a good ion crowding around ether oxygen is sustained for a fairly wide composition range. For electrical transport, the majority of Li^+ ions thus may move through coupling, i.e., by shifting coordination with ether oxygen as discussed earlier [9][2]. It is also important to mention that ion transport associated with ion-chain coupling is a slow process [13] therefore, a significant increase in conductivity is not observed for low LATP content.

(iii) For high LATP content (50-70 LATP), the E_O value appears to almost saturate/decrease. Further with a decrease in O/Li ratio creates excessive crowding of Li+ ions around ether oxygen and thus possibly leads to detachments of Li^+ ions from the polymer chain. Thus, free (decoupled) Li^+ ions may take vacant states available on the surface or bulk of NASICON. In such a situation when electric

field is applied, Li^+ ions prefer to move through polymer–grain interface (using surface states) as well as through LATP grains. A transport through LATP grains is also complemented by the comparable low activation energy of electrical transport (Chapter 3, Fig 3.11a) of the second phase to that of bulk LATP. A significant increase in Li^+ ion transport number and ionic mobility for compositions in this region does compliment the same.

5.2 X-Ray photoelectron Spectroscopy (XPS)

In the previous section, we attempt to understand ionic transport in Na^+ and Li^+ ion composites using X-ray absorption spectroscopy. Analyzing the K-edge energy of ether oxygen of polyethylene oxide (PEO) polymer, a possible decoupling of salt cations from the ether oxygen of the polymer matrix is proposed, particularly at the higher NASICON content. Therefore, these cations are likely to take the pathways provided by NASICON via (i) surface or (ii) bulk, for electrical transport. However, it was realized to also complement the XANES results by other similar technique to establish an evidence-based mechanism. Thus, the section discusses cation polymer chain interaction using X-ray photoelectron spectroscopy (XPS).

In the current section, the XPS of the compositions (with ratio in wt%) for Li^+ and Na^+ ion systems viz. (i) $5LiCF_3SO_3$-$95[PEO_{1-x}LATP_x]$ where $0 \leq x \leq 0.7$, and $Li_{1.3}Al_{0.7}Ti_{1.3}(PO_4)_3$ termed as LATP (ii) $63NZSP$-$37[PEO_{1-y}NaI_y]$ where $y = 0.03–0.13$, and $Na_3Zr_2Si_2PO_{12}$ termed as NZSP is discussed.

XPS spectra were analyzed using CasaXPS software (version 2.3.19) using U 2 Tougaard background correction. Asymmetric Lorentzian profiles, defined in CasaXPS of form LA(α, β, m) where α and β define the spread of the tail on either side of the Lorentzian component and the parameter m specifies the width of the Gaussian used to convolute the Lorentzian curve, were used for each component. The O 1s spectra of the composites were best fit with line-shapes of asymmetric peak-shape LA(1.53, 243) for throughout composition. Peak fitting parameters for O 1s spectra are presented in Table 5.2 and Table 5.3 for system viz. (i) $5LiCF_3SO_3$-$95[PEO_{1-x}LATP_x]$ and (ii) $63NZSP$-$37[PEO_{1-y}NaI_y]$, respectively.

Table 5.2 Peak position and their relative peak area ratio correspond to deconvoluted O 1s spectra for composites $5LiCF_3SO_3$-$95[PEO_{1-x}LATP_x]$ and pristine LATP. Here * refers peak that are difficult to identify due to low content and overlapping. The residual standard deviation for all the fitting was found to be ~1 eV.

	Peak												Peak area ratio		
Composition	O 1s (1)			O 1s (2)			O 1s (3)			O 1s (4)			$\frac{O\ 1s\ (3)}{O\ 1s\ (4)}$	$\frac{O\ 1s\ (1)}{O\ 1s\ (3)}$	$\frac{O\ 1s\ (1)}{O\ 1s\ (4)}$
	B.E. (eV)	β(eV)	Area	B.E. (eV)	β(eV)	Area	B.E. (eV)	β(eV)	Area	B.E. (eV)	β(eV)	Area			
0 LATP	533.21	3.06	7286.88	535.88	3.06	1441.76	-	-	-	-	-	-	-	-	-
10 LATP	532.93	3.09	10124.21	535.40	3.89	2952.50	*	*	*	*	*	*	-	-	-
30 LATP	534.21	4.72	11108.07	*	*	*	532.14	2.11	5532.81	533.29	2.23	5214.60	1.06	2.00	2.13
40 LATP	535.08	3.71	3932.70	*	*	*	532.08	2.60	9957.77	533.64	3.06	7019.14	1.41	0.40	0.56
50 LATP	535.84	3.40	2756.73	*	*	*	532.04	2.50	7966.14	533.53	2.96	6759.60	1.17	0.35	0.40
60 LATP	535.78	4.37	5174.47	*	*	*	531.78	3.31	7569.37	533.07	3.54	5749.98	1.31	0.68	0.89
70 LATP	535.70	4.15	2672.51	*	*	*	531.82	3.21	7646.47	533.29	4.39	9390.77	0.81	0.34	0.28
LATP	-	-	-	-	-	-	531.67	3.16	7274.13	533.74	4.92	6450.53	1.12	-	-

Table 5.3 Peak position and their relative peak area ratio correspond to deconvoluted O 1s spectra for composites 63NZSP-[$PEO_{1-y}NaI_y$] and pristine NZSP. The residual standard deviation for all the fitting was found to be~1eV.

	Peak									Peak area ratio		
Composition (y)	O 1s (1)			O 1s (2)			O 1s (3)			$\frac{O\ 1s\ (2)}{O\ 1s\ (3)}$	$\frac{O\ 1s\ (3)}{O\ 1s\ (1)}$	$\frac{O\ 1s\ (3)}{O\ 1s\ (2)}$
	B.E. (eV)	β(eV)	Area	B.E. (eV)	β(eV)	Area	B.E. (eV)	β(eV)	Area			
0.03	532.12	3.38	7283.30	534.02	2.74	2700.33	536.13	3.18	1647.55	1.63	3.00	4.93
0.07	532.36	3.80	4034.70	534.75	3.70	1525.35	536.01	4.60	1330.94	1.14	2.64	3.03
0.11	532.11	3.69	1152.98	534.13	3.01	514.26	536.15	3.19	398.94	1.29	0.87	1.13
0.13	532.96	2.86	3127.99	534.63	2.95	4266.09	536.16	3.90	2617.61	1.63	0.73	1.79
NZSP	-	-	-	534.61	2.83	10914.16	536.05	4.70	14107.88	1.33	-	-

5.2.1 5LiCF$_3$SO$_3$-95[PEO$_{1-x}$LATP$_x$] system

XPS spectra (resolution of 0.1 eV) for composites of 5LiCF$_3$SO$_3$-95[PEO$_{1-x}$LATP$_x$] and LATP were obtained, and the deconvoluted spectra assigned with various peaks are shown in Fig. 5.7. The hydrocarbon C 1s peak at 285 eV was used as a reference value for the binding energy calibration. The trend of O 1s binding energy for composites with LATP was studied by taking the sample 95PEO-5LiCF$_3$SO$_3$ (x = 0) as a reference. As evident, the oxygen spectra of x = 0 sample is deconvoluted into two peaks O 1s (1) and O 1s (2), which are assigned to ether oxygen of PEO (CH$_2$-CH$_2$-O-) and oxygen of $CF_3SO_3^-$ units, respectively, in agreement with the earlier reported [14]. A similar deconvoluted peak is also observed for sample with small amount of LATP (x = 0.1, 0.2) (Fig. 5.7b).

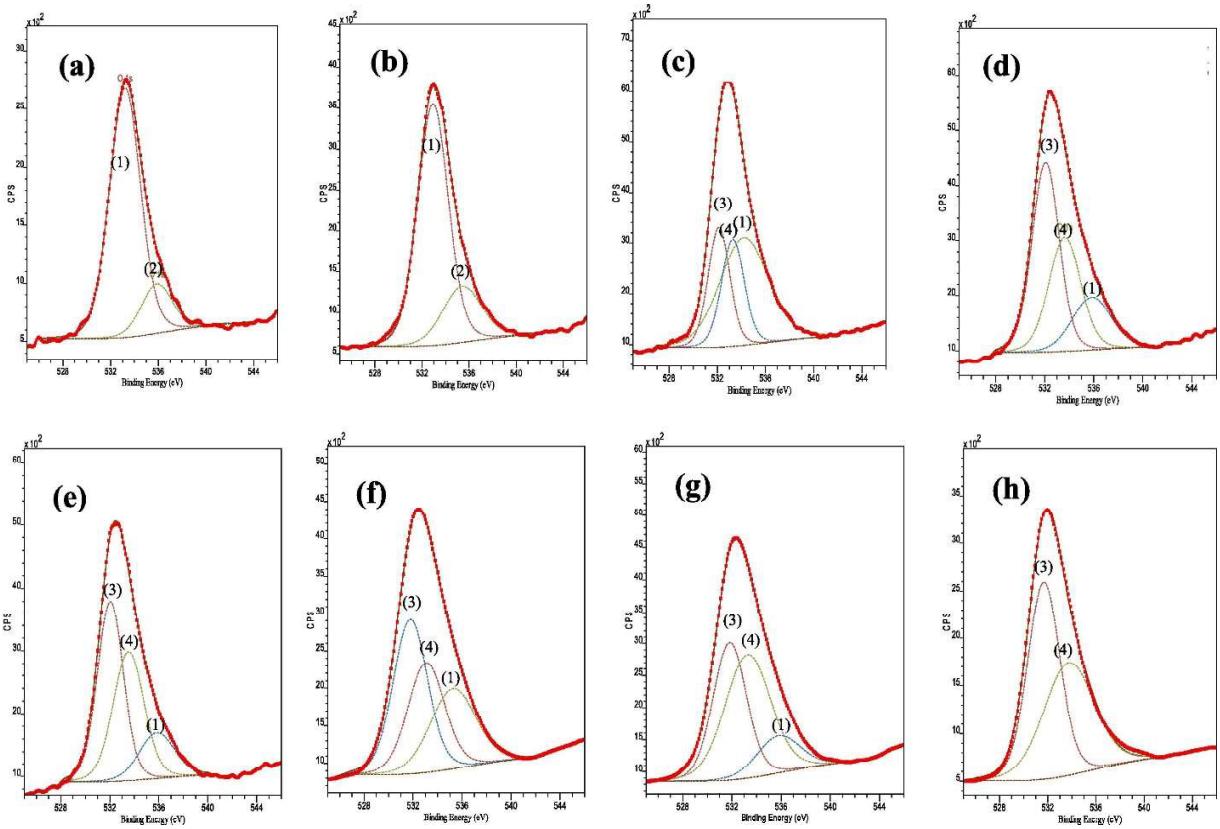

Figure 5.7 *Core level (O 1s) XPS spectra with deconvoluted peaks for composite (a) x = 0, (b) x = 0.1, (c) x = 0.3, (d) x = 0.4, (e) x = 0.5, (f) x = 0.6, (g) x = 0.7 and (h) Pristine LATP. The complete core level spectrum is represented by dotted red colour line. Further, the convoluted spectra is represent by brown colour line. Instrument resolution: 0.01 eV.*

However, for further high LATP content, the O 1s spectra for composites with x = 0.3–0.7 appear to be deconvoluted into three peaks, where the peaks are assigned keeping pristine LATP deconvoluted peaks of O 1s spectra as reference. As observed in Fig. 5.7h, the O 1s spectrum of LATP [15] is deconvoluted into two peaks O 1s (3) and O 1s (4), which may be assigned to the oxygen of tetrahedra $(PO_4)^-$ and octahedra $(TiO_6)^-$ units, respectively.

Considering peak positions and peak area ratio of (i.e. O 1 s of octahedra to tetrahedra) LATP sample (Table 5.2), the first two deconvoluted peaks (Fig. 5.7c–g) observed at lower binding energy for composite with x = 0.3-0.7 are respectively assigned to LATP (i.e. O 1s (3) and O 1s (4)). The observed third peak at higher binding energy is again assigned to O 1s (1) after considering its peak area. However, the O 1s (2) peak from $CF_3SO_3^-$ units probably overlaps with the O 1s (1) peak of $–CH_2CH_2$-O-. Importantly, any shift in O 1s (1) peak position would correspond to ether oxygen interacting with cations (Li^+) thus infer about ion chain coupling or decoupling.

The binding energy correspond to O 1s (1) is plotted against LATP content (Fig. 5.8). As evident, the binding energy exhibits a shift to higher values with LATP content. Such a shift is monotonic and readily suggests the coupling of cations with ether oxygen of PEO. This stronger interaction of Li^+ ions with ether oxygen is expected.

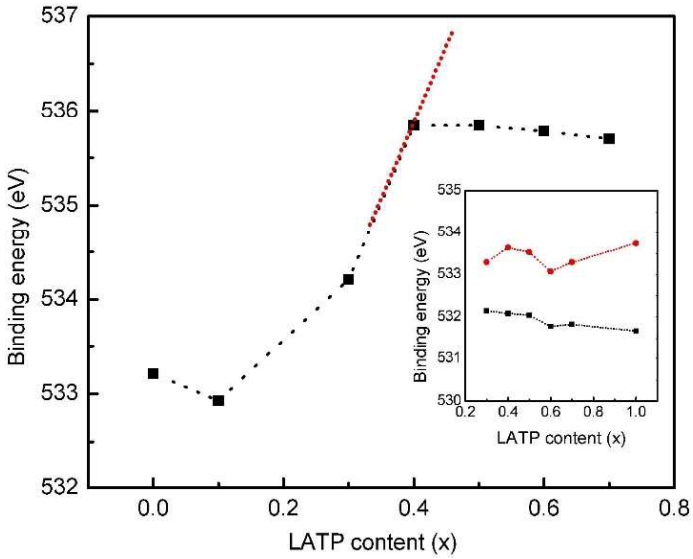

Figure 5.8 *Binding energy (O 1s) corresponding to ether oxygen of PEO with LATP variation in $5LiCF_3SO_3$-$95[PEO_{1-x}LATP_x]$ composites. Dotted lines denote deviation from the monotonic rise of binding energy. Inset: Binding energy of LATP oxygens (O 1s (3) and O 1s (4)) with its variation in the matrix. Instrument resolution: 0.01 eV.*

Since LATP substitution in the matrix is on the cost of PEO, this leads to a systematic decrease in the number of ether oxygens and hence O/Li ratio. Thus with a gradual decrease of O/Li ratio from 67/1 (x = 0) to 40/1 (x = 0.4), the binding energy shows an expected gradual rise. Surprisingly, with a further decrease of O/Li ratio to 20/1 (x = 0.7), the binding energy does not exhibit expected rise (shown by dotted line), instead exhibits a saturation. These results strongly suggest decoupling of Li^+ ions from ether oxygen of PEO, particularly when LATP content reaches to a significantly high volume fraction. Inset of Fig. 5.8 depicts binding energy correspond to O 1s (3) and O 1s (4) against LATP content. LATP addition in the matrix leads to no change in the binding energies of its own oxygens. That further suggests no distortion in the tetrahedra $(PO_4)^-$ and octahedra $(TiO_6)^-$ units in the LATP, when it exists with polymer. Previous XANES investigations on these composites also complement these findings, where the K-edge energy corresponding to ether oxygen also follows similar trends as that of the O 1s energy in the present case. Thus, the XPS results also strongly suggest the decoupling of Li^+ ions at higher NASICON content. Thus for high NASICON content in the matrix, the ionic transport is via the NASICON surface or grain interior (bulk).

63NZSP-37[$PEO_{1-y}NaI_y$] system

In case of Na^+ ion system with composition 63NZSP-37[$PEO_{1-y}NaI_y$] and pristine NZSP, the deconvoluted XPS spectra assigned with various peaks corresponding to O 1s are shown in Fig. 5.9. Since, NZSP is in large amount; in this case the deconvoluted peak for O 1s is assigned by considering O 1s spectra of NZSP as a reference. As shown in Fig. 5.9e, the deconvoluted two peaks, viz O 1s (2) and O 1s (3), may be respectively assigned to $(Si,P)O_4$ tetrahedra and ZrO_6 octahedra unit [16].

Considering the peak area ratio and binding energy of NZSP units (Table 5.2), the three deconvoluted peaks (Fig. 5.9b-e) of composites may again be assigned as O 1s (1), O 1s (2) and O 1s (3), corresponds to ether oxygen of $–CH_2-CH_2-O-$, $(Si,P)O_4$ tetrahedra and ZrO_6 octahedra units, respectively. In view of cation interaction with ether oxygen of PEO, the O 1s (1) binding energy is plotted against salt content (Fig. 5.10).

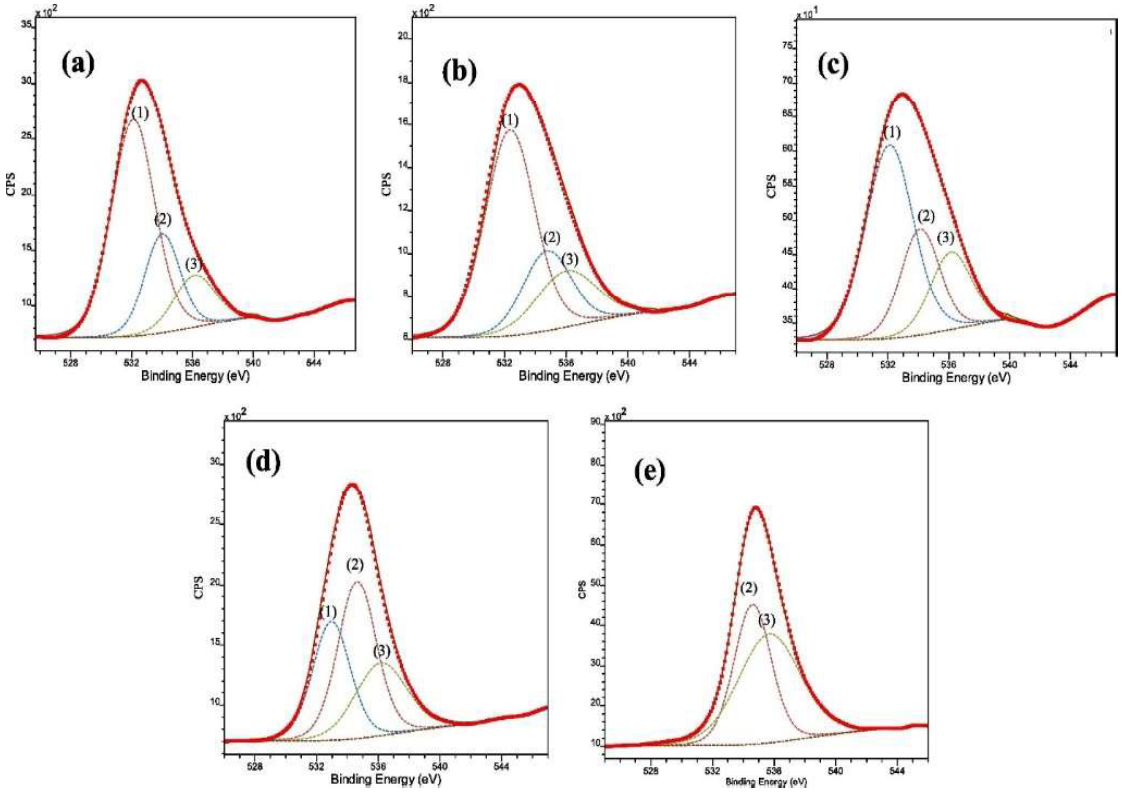

Figure 5.9 *Core level (O 1s) XPS spectra with deconvoluted peaks for 63NZSP-[$PEO_{1-y}NaI_y$] composite (a) y = 0.03, (b) y = 0.07, (c) y = 0.11 (d) y = 0.13 and (e) pristine NZSP. Similar to Fig. 7, the complete core level spectrum is represented by dotted red colour line and convoluted spectra is represent by brown colour line. Instrument resolution: 0.01 eV.*

With NaI variation (on the cost of PEO), shifting of binding energy towards higher side is expected, as O/Na ratios decreases from 30/1 (y = 0.03) to 6/1(y = 0.13). On the contrary, the O 1s (1) binding energy remains almost constant that readily suggests a saturation limit of Na^+ ion-ether oxygen interaction. Thus, added cations do not further accumulate around ether oxygens. Similar to the earlier case for Li^+ ion system, it is again an evidence of decoupling of Na^+ ion from the ether oxygen when the NASICON content is high in the matrix. Thus, in general, for Li^+/Na^+ ion conducting polymer-NASICON system, presence of NASICON in large amount leads to cation detachment from polymer matrix. Inset of Fig. 5.10 depicts binding energy corresponding to O 1s (2) and O 1s (3) against NZSP content. The constant value of binding energy with NZSP content suggests undistorted octahedral and tetrahedral sites of NZSP crystallites in hybrid composites. Results for both the above systems are

certainly complimented by XANES of O-K edge spectra where similar trend is witnessed in the K-edge energy of ether oxygen as discussed in earlier. XPS investigations thus give insight into the interaction of cations with polymer matrix that may be extremely useful to probe conductivity mechanism.

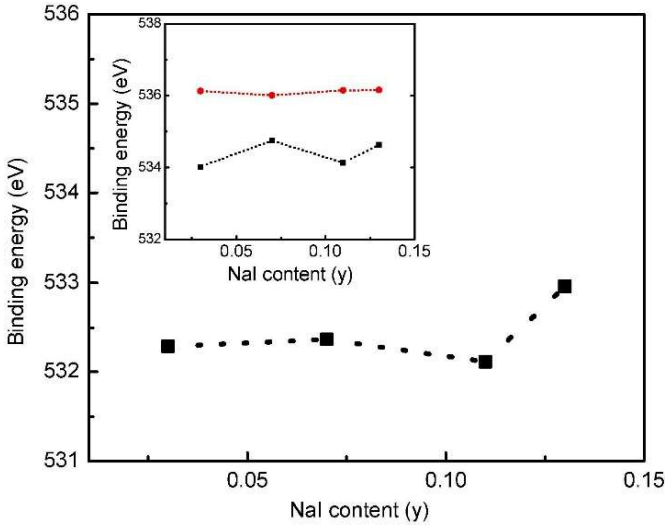

Figure 5.10 *Binding energy (O 1s) corresponding to ether oxygen of PEO with salt concentration variation in 63NZSP-[$PEO_{1-x}NaI_x$] composites. Inset: Binding energy for NZSP oxygens (O 1s (2) and O 1s (3)) with its variation in the matrix. Instrument resolution: 0.01 eV.*

5.3 Ion transport at glass transition (T_g) of polymer

To explore more evidence of the role of polymer chains on electrical transport, low temperature electrical conductivity for the two series of samples is measured and shown in Fig. 5.11 a and b. An attempt was to comprehend the behavior of conductivity below the glass transition of PEO ($T < T_g$) where the chain flexing is expected to freeze. Fig. 11a shows conductivity versus temperature for LATP-PEO films as a function of NASICON content in the matrix.

With the decrease in temperature, the conductivity gradually decreases. Interestingly, as the temperature reaches below T_g, the conductivity falls apparently for the sample without NASICON content. This readily suggests the role of ion chain coupling in electrical transport. Even for $T < T_g$ the cations are still coupled with ether oxygens but unable to contribute to electrical transport in absence of chain flexing. The behavior of conductivity is however

different for high NASICON content samples. Interestingly, the conductivity below freezing of polymer does not undergo a drastic fall but to surprise, it tends to saturate. This is important evidence of decoupling of cations from polymer chains for large NASICON content samples. The cations possibly tend to move through NASICON grains/surface states and polymer freezing does not affect the conductivity. The saturation in the conductivity at further lower temperatures is due to poor thermal activated behavior of mobile Li^+ ion in NASICON grains. Similar evidence of decoupling is apparent in the case of Na^+ ion systems as well (Fig. 5.11b).

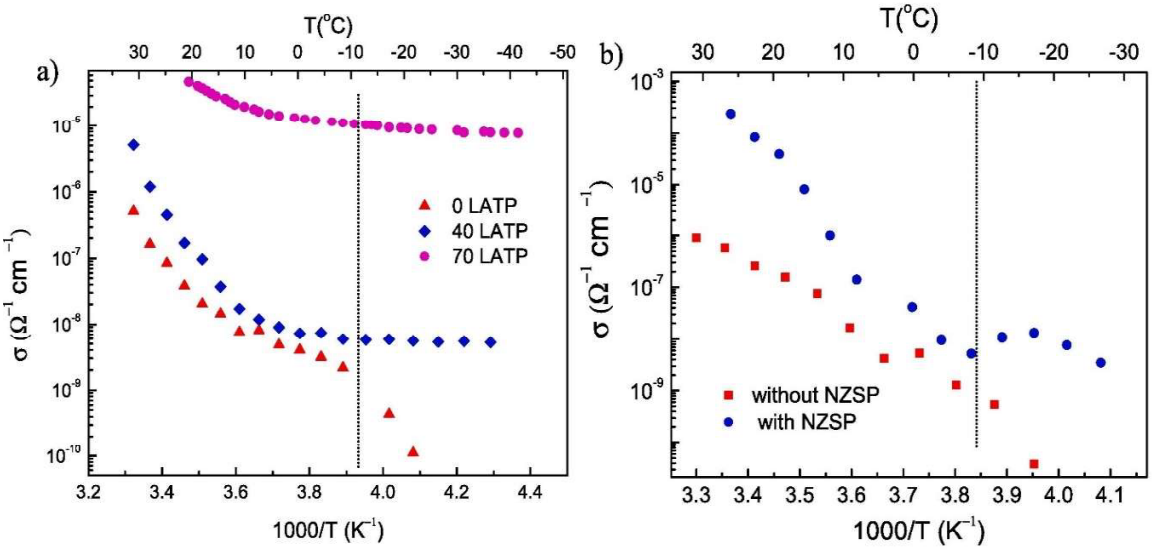

Figure 5.11 *Temperature dependent ionic conductivity for samples with NASICON and without NASICON content in respective polymer matrix below room temperature (220–300 K) for (a) LATP-PEO-$LiCF_3SO_3$ system and (b) NZSP-PEO-NaI system.*

5.4 Generalized Ion Transport Mechanism for Li^+/Na^+ ion composites

Above findings from XPS and XANES spectra the following ion transport mechanism supports the cation transport in the polymer-NASICON hybrid composites.

(i) The rise in O 1s (XPS) or Eo (XANES) energy corresponding to ether oxygen of polymer chain refers to cation accumulation (or crowding) in the polymer matrix. Thus, for low NASICON content in the polymer matrix, cations stay in polymer and the vicinity of ether oxygen. This readily suggests that coupling is likely to play an important role in ion transport. It is also evident from the composition dependence of conductivity that for low NASICON content samples this rise is not significant. As the

O/Li ratios decrease (from 67/1 to 40/1), conductivity rise is rather moderate with NASICON content. This is essentially attributed to the ions chain coupling mechanism which is a very slow process [17], [18], [2].

(ii) For higher NASICON content, when O/M (M = Na^+ or Li^+) ratio decreases, O 1s (XPS), as well as Eo (XANES) energy, remains almost constant/decreases for both systems that readily suggest decoupling of cations from ether oxygen of PEO. Thus for such compositions, ion chain coupling may not be the preferred mechanism for ionic transport. Interestingly, for the higher concentration of NASICONs conductivity rise is quite significant that readily suggest the role of conductive grains in providing pathways for electrical transport.

With the above finding from XANES and XPS spectra, a schematic ion transport mechanism in polymer-NASICON hybrids composite is shown in Fig. 5.12. As in Fig. 5.12, the composite with lower NASICON exhibits cation-polymer chain coupling, and thus polymer chain relaxation process facilitate ions transport in these composites. While the composite with higher NASICON content exhibits decoupling of cations from polymer chain. Thus, cations transport through bulk or surface state of NASICON facilitates the movement of the ions.

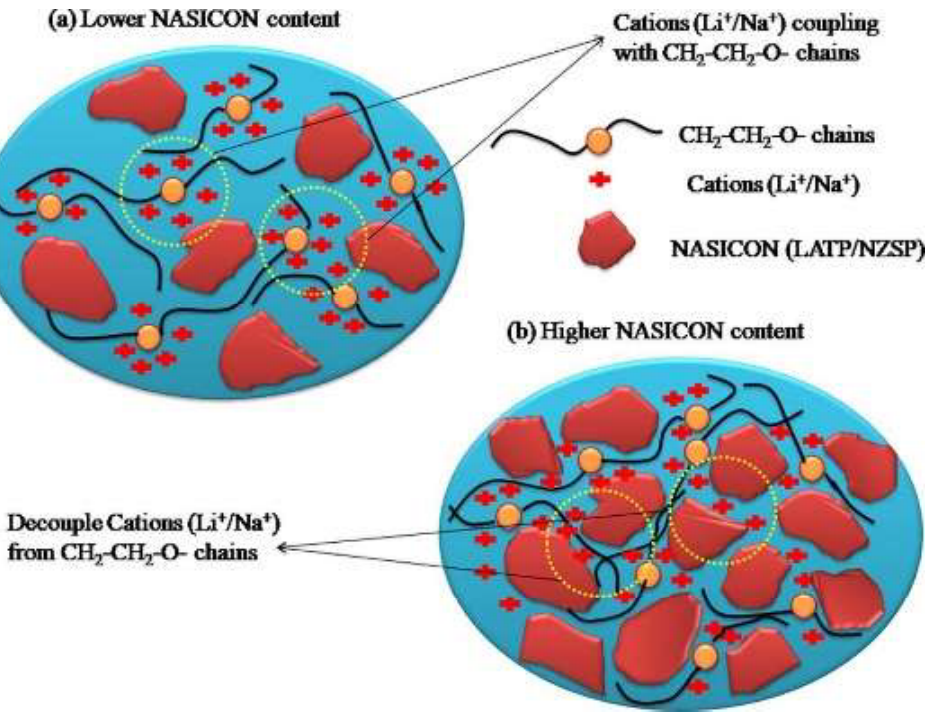

Figure 5.12 *Generalized ion transport mechanism in polymer-NASICON hybrid composites.*

5.5 Summary

(i) Tentative understanding of the mechanism of conductivity in chapters 3 and 4 required evidence of ionic motion via NASICON grains or polymer regions. XANES and XPS results revealed interesting findings of cation interaction with the polymer chains in Na^+ and Li^+ ion based NASICON-polymer composites. This has provided a good understanding of the mechanism.

(ii) Mechanism reveals that the role of NASICON or polymer in supporting the electrical transport depends on whether ions are coupled/detached with ether oxygen of the PEO. Coupling of cations with ether oxygen at lower NASICON content, and decoupling at high content decide the ion pathways. Cation coupling with ether oxygen of polymer is evident in XANES as well as XPS for lower NASICON content. Thus, ion chain relaxation may be the preferred mechanism for ion transport.

(iii) It is quite evident that for the larger content of these nanocrystallites in the matrix, there is a decoupling of cations from polymer chains. For the composites with higher NASICON content, the ions transport mechanism is thus facilitated by surface states or bulk of the NASICON. For low NASICON content composites, these active fillers still play important role in creating amorphous phase, and providing mechanical strength.

(iv) Electrical transport studies, particularly, conductivity investigated in previous chapters and the conductivity near T_g of the polymer further reveal that such decoupled cations move through pathways provided by NASICON grains. Therefore, the conductivity of active fillers dictates the electrical transport.

Reference:

[1] J. Mindemark, M.J. Lacey, T. Bowden, D. Brandell, Beyond PEO—Alternative host materials for Li+-conducting solid polymer electrolytes, Prog. Polym. Sci. 81 (2018) 114–143. https://doi.org/10.1016/j.progpolymsci.2017.12.004.

[2] D. Golodnitsky, E. Strauss, E. Peled, S. Greenbaum, Review—On Order and Disorder in Polymer Electrolytes, J. Electrochem. Soc. 162 (2015) A2551–A2566. https://doi.org/10.1149/2.0161514jes.

[3] B. Ravel, M. Newville, ATHENA, ARTEMIS, HEPHAESTUS: Data analysis for X-

ray absorption spectroscopy using IFEFFIT, in: J. Synchrotron Radiat., 2005: pp. 537–541. https://doi.org/10.1107/S0909049505012719.

[4] A.K. Yadav, S.M. Haque, R. De, M.A. Ahmed, V. Srihari, M. Gupta, D.M. Phase, S. Bandyopadhyay, S.N. Jha, D. Bhattacharyya, Local Structure Investigation of Mn- and Co–Doped TiO2 Thin Films by X-Ray Absorption Spectroscopy, ChemistrySelect. 2 (2017) 11012–11024. https://doi.org/https://doi.org/10.1002/slct.201702263.

[5] D.C. Koningsberger, B.L. Mojet, G.E. Van Dorssen, D.E. Ramaker, XAFS spectroscopy; fundamental principles and data analysis, Top. Catal. 10 (2000) 143–155. https://doi.org/10.1023/a:1019105310221.

[6] J. Kikuma, B.P. Tonner, XANES spectra of a variety of widely used organic polymers at the C K-edge, J. Electron Spectros. Relat. Phenomena. 82 (1996) 53–60. https://doi.org/10.1016/s0368-2048(96)03049-6.

[7] J.B. Kortright, J. Sun, R.K. Spencer, X. Jiang, R.N. Zuckermann, Oxygen K edge scattering from bulk comb diblock copolymer reveals extended, ordered backbones above lamellar order disorder transition, J. Phys. Chem. B. 121 (2017) 298–305. https://doi.org/10.1021/acs.jpcb.6b09925.

[8] J. Kikuma, B.P. Tonner, XANES spectra of a variety of widely used organic polymers at the C K-edge, 82 (1996) 53–60.

[9] S.B. Aziz, T.J. Woo, M.F.Z. Kadir, H.M. Ahmed, A conceptual review on polymer electrolytes and ion transport models, J. Sci. Adv. Mater. Devices. 3 (2018) 1–17. https://doi.org/10.1016/j.jsamd.2018.01.002.

[10] Y. Zhao, Z. Huang, S. Chen, B. Chen, J. Yang, Q. Zhang, F. Ding, Y. Chen, X. Xu, A promising PEO/LAGP hybrid electrolyte prepared by a simple method for all-solid-state lithium batteries, Solid State Ionics. 295 (2016) 65–71. https://doi.org/10.1016/j.ssi.2016.07.013.

[11] M. Brown, R.E. Peierls, E.A. Stern, White lines in x-ray absorption, Phys. Rev. B. 15 (1977) 738–744. https://doi.org/10.1103/PhysRevB.15.738.

[12] R. Singh, M. Gupta, D.M. Phase, S.K. Mukherjee, Phase growth analysis of sputtered

TiO2 thin films at low oxygen partial pressures using XANES and XRR, Mater. Res. Express. 6 (2019) 116449. https://doi.org/10.1088/2053-1591/ab4e3f.

[13] M.A. Ratner, D.F. Shriver, Ion Transport in Solvent-Free Polymers, Chem. Rev. 88 (1988) 109–124. https://doi.org/10.1021/cr00083a006.

[14] D. Martin-Vosshage, B.V.R. Chowdari, XPS studies on (PEO)nLiCF3SO3 and (PEO)nCu(CF3SO3)2 polymer electrolytes, Electrochim. Acta. 40 (1995) 2109–2114. https://doi.org/https://doi.org/10.1016/0013-4686(95)00148-8.

[15] P. Bhanja, C. Senthil, A.K. Patra, M. Sasidharan, A. Bhaumik, NASICON type ordered mesoporous lithium-aluminum-titanium-phosphate as electrode materials for lithium-ion batteries, Microporous Mesoporous Mater. 240 (2017) 57–64. https://doi.org/10.1016/j.micromeso.2016.11.005.

[16] S. Wang, H. Xu, W. Li, A. Dolocan, A. Manthiram, Interfacial Chemistry in Solid-State Batteries: Formation of Interphase and Its Consequences, J. Am. Chem. Soc. 140 (2018) 250–257. https://doi.org/10.1021/jacs.7b09531.

[17] F. Croce, R. Curini, a. Martinelli, L. Persi, F. Ronci, B. Scrosati, R. Caminiti, Physical and Chemical Properties of Nanocomposite Polymer Electrolytes, J. Phys. Chem. B. 103 (1999) 10632–10638. https://doi.org/10.1021/jp992307u.

[18] S.K. Fullerton-Shirey, J.K. Maranas, Effect of LiClO4 on the Structure and Mobility of PEO-Based Solid Polymer Electrolytes, Macromolecules. 42 (2009) 2142–2156. https://doi.org/10.1021/ma802502u.